

Increase of saturation current in unipolar field-effect transistor due to bulk electric conductance of organic semiconductor

Cite as: AIP Advances 9, 025313 (2019); <https://doi.org/10.1063/1.5088117>

Submitted: 08 January 2019 . Accepted: 12 February 2019 . Published Online: 25 February 2019

L. V. Govor , and J. Parisi



View Online



Export Citation



CrossMark

ARTICLES YOU MAY BE INTERESTED IN

[Monte Carlo-based simulation of x-ray phase-contrast imaging for diagnosing cold fuel layer in cryogenic implosions](#)

AIP Advances 9, 025311 (2019); <https://doi.org/10.1063/1.5087615>

[Deterministic generation and switching of dissipative Kerr soliton in a thermally controlled micro-resonator](#)

AIP Advances 9, 025314 (2019); <https://doi.org/10.1063/1.5080128>

[Strain-dependence of \$\chi^{\(2\)}\$ in thin film barium strontium titanate](#)

AIP Advances 9, 025312 (2019); <https://doi.org/10.1063/1.5055731>

AVS Quantum Science

Co-published with AIP Publishing



Coming Soon!

Increase of saturation current in unipolar field-effect transistor due to bulk electric conductance of organic semiconductor

Cite as: AIP Advances 9, 025313 (2019); doi: 10.1063/1.5088117

Submitted: 8 January 2019 • Accepted: 12 February 2019 •

Published Online: 25 February 2019



View Online



Export Citation



CrossMark

L. V. Govor^{a)}  and J. Parisi

AFFILIATIONS

Institute of Physics, Carl von Ossietzky University of Oldenburg, D-26111 Oldenburg, Germany

^{a)}Email: leonid.govor@uni-oldenburg.de

ABSTRACT

We considered an organic field-effect transistor (OFET) based on a squaraine (SQ) fiber, where the electric conductance of the accumulation channel is comparable with the bulk conductance of the SQ fiber. Each of the measured output and transfer current-voltage characteristics was decomposed into two components, representing the conductance of the accumulation channel and the bulk. We present in detail, how the bulk conductance of the fiber can transform the output characteristics of the unipolar OFET. For positive drain and gate voltage, the hole injection from the drain always takes place when a drain voltage is applied. Depending on the ratio between the electron density (n_s) injected from the source into accumulation channel and the hole density (p_b) injected from the drain into the bulk, the saturation current of the unipolar OFET is constant ($p_b < n_s$) or exhibits increase ($p_b \geq n_s$).

© 2019 Author(s). All article content, except where otherwise noted, is licensed under a Creative Commons Attribution (CC BY) license (<http://creativecommons.org/licenses/by/4.0/>). <https://doi.org/10.1063/1.5088117>

I. INTRODUCTION

Organic field-effect transistors (OFETs) are important building blocks for flexible electronic applications, particularly, considering their low-cost fabrication and flexibility over large areas.^{1,2} The most common configuration of an OFET contains an organic semiconductor, upon which three metal electrodes are deposited. The gate electrode (G) is electrically insulated from the semiconductor via the dielectric layer, but both the drain (D) and source (S) electrodes contact immediately the semiconductor. The S electrode is usually grounded and the voltage applied to the G electrode (V_g) and the D electrode (V_d). When only a small voltage V_d is applied between the D and S electrodes upon $V_g=0$, the measured current becomes minimal, and the OFET is in the “off” state. If, for example, a positive voltage V_g is applied between the G and S electrodes, the electrons are induced at the semiconductor-dielectric interface (accumulation channel). The current between the D and S electrodes increases, and the OFET is in the “on” state.

For the voltage regime $0 \leq V_d < V_g - V_{te}$ (V_{te} is the threshold voltage for electron accumulation), the OFET operates in the linear regime of the unipolar electron conductance, and the current in the accumulation channel is given by^{3,4}

$$I_d = \frac{WC_i}{2L} \mu_e [2(V_g - V_{te}) - V_d] V_d, \quad (1)$$

where I_d is the drain current, μ_e the field-effect electron mobility, W the channel width, L the channel length, and C_i the capacitance per unit area of the insulator layer. For the voltage regime $0 < V_g - V_{te} < V_d < V_g - V_{th}$ (V_{th} is the threshold voltage for hole accumulation), the gate electric field at the D electrode becomes zero, and the accumulation channel is pinched off. In this case, the OFET operates in the saturation regime of the unipolar electron conductance, and the channel current is given by^{3,4}

$$I_d = \frac{WC_i}{2L} \mu_e (V_g - V_{te})^2. \quad (2)$$

The current in the ambipolar OFET can be caused by the simultaneous injection of electrons and holes from source and drain, respectively. The latter process depends on the ratio between the voltages V_g and V_d . If $V_{te} \leq V_g - V_{th} \leq V_d$, the transistor operates in the ambipolar regime, where the gate potential is more negative compared to the drain one. In this case, electrons injected from the S electrode cannot be accumulated in the pinched-off part of the channel, and holes are injected from the D electrode into the channel. As a result, both electrons and holes are present in the accumulation channel, giving rise to an increase of the drain current in the $I_d(V_d)$ characteristic. The accumulation channel can be considered as superposition of the saturated electron channel (with length L_e) and the saturated hole channel (with length L_h).^{3,4} The total channel length is $L = L_e + L_h$. It is assumed that at the point, where both channels meet, an infinite recombination rate of electrons and holes takes place. Using Eq. (2), the ambipolar behavior of the OFET can be described as^{3,4}

$$I_d = \frac{WC_i}{2L} [\mu_e(V_g - V_{te})^2 + \mu_h(V_d - (V_g - V_{th}))^2], \quad (3)$$

where μ_h is the hole mobility.

For the disordered organic semiconductors, Smits et al.⁵ have developed a model describing the charge transport in disordered ambipolar OFETs. In this case, the lowest unoccupied molecular orbital (LUMO) and the highest occupied molecular orbital (HOMO) bands can not be described as two delocalized energy bands separated by a gap. Rather, the bands can be described as bands where the localized energetic states are distributed. In this model, the electrical transport is described as variable-range hopping in an exponential density of states (including the percolation theory). The electrons move through the unoccupied density of states corresponding to the LUMO levels, and the holes move through the occupied density of states corresponding to the HOMO levels. It is shown that the latter model can be applied to a wide range of bias conditions and can give a fair description of the unipolar and ambipolar behavior of the OFETs.^{5,6}

At this point, it is interesting to know the following: If the initial bulk conductance of the semiconductor ($V_g=0$) in the OFET described by the power law $I_d \sim V_d^\beta$ is comparable (or larger) than that of the accumulation channel in the saturation regime, is it possible that it leads to the increase of the saturation current (similar to the ambipolar behavior) and the output characteristic can be described by Eq. (4)?

$$I_d = \frac{WC_i}{2L} \mu_e(V_g - V_{te})^2 + \alpha b V_d^\beta, \quad (4)$$

where α is the fraction of the bulk current in the total measured current, b and β are parameters describing the bulk conductance. It is evident that Eq. (4) is evaluated from Eq. (3), where the second term describing the ambipolar behavior of the OFET is replaced with a term describing the bulk conductance. In other words, the first term in Eq. (4) is the current flowing through the accumulation channel and the second one that through the bulk. To find an answer, we have studied an OFET based on the squaraine fiber, the initial bulk conductance of which was comparable with the conductance of the

accumulation channel of the OFET. We show, how these two currents can be separated. For small values of V_d , the output characteristics of the devices studied show a linear regime, but, for large values of V_d , a saturation current becomes larger. The experimental output characteristics were approximated with the standard Eqs. (1)–(3), with equations proposed by Smits et al.⁵ and with Eq. (4). We found that the best fit was achieved with the Eq. (4). That means, the bulk conductance of the SQ fiber in the OFET can give rise to the increase of the saturation current, if its value is comparable (or larger) with that of the accumulation channel. An understanding of this effect is important to prevent an incorrect interpretation of the charge transfer in the ambipolar OFET.

II. EXPERIMENT

For fabrication of the OFET, we have used the fibers of 2,4-bis[4-(N,N-diisobutylamino)-2,6-dihydroxyphenyl] squaraine (SQ) (empirical formula $C_{32}H_{44}N_2O_6$) purchased from Aldrich. Squaraine is commonly used as a donor material in organic solar cells.⁷ The SQ fibers were formed with a method which we have developed earlier,⁸ where the solution of squaraine in chlorobenzene (4 mg/mL) was used. Briefly, via pinning the solution droplet edge on the glass substrate and following solvent evaporation from the droplet, the SQ fibers were formed at the droplet edge. For the OFET fabrication, we have used fibers with the following dimensions: length 100–300 μm , width 2–5 μm , and thickness 2–5 μm . In order to achieve an ohmic contact with the SQ fiber which has a HOMO level estimated to be -5.3 eV,^{9,10} we have chosen gold as the

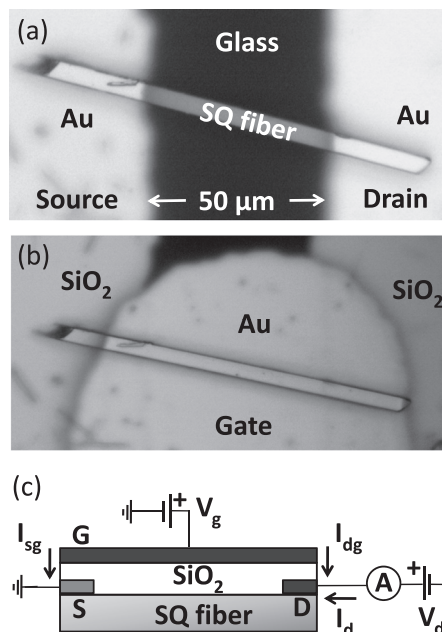


FIG. 1. (a) and (b) Optical micrograph of a SQ fiber with a length of 130 μm , width of 5 μm , and thickness of 5 μm after deposition of S, D, and G electrodes. (c) Schematic representation of an OFET and the measuring circuit. All abbreviations and symbols are explained in the text.

metallic material of the S and D electrodes (100 nm thick). The corresponding LUMO of squaraine was estimated to be -3.4 eV in Ref. 9 and -3.6 eV in Ref. 10, respectively. A typical SQ fiber with deposited S and D electrodes is presented in Fig. 1(a). The distance between the S and D electrodes amounts to $50 \mu\text{m}$. Afterwards, the SiO_2 layer with a thickness of 390 nm and the G electrode (gold) with a thickness of 100 nm were electron beam deposited, see Fig. 1(b). Electrical characterization of each sample was carried out by measurement of the output curves for the drain voltage V_d from 0 to ± 20 V, and the transfer curves for the gate voltage V_g from 0 to ± 50 V. A subfemto-Ampere meter source (Keithley 6430) was used to apply V_d , and the current I_d has been measured. A high-impedance electrometer (Keithley 6517A) was taken to apply V_g . A schematic representation of the OFET studied and the measuring circuit are illustrated in Fig. 1(c). In total, eight samples have been analyzed. We only present results obtained from one representative sample, because the other ones showed similar characteristics. The main difference between the samples consisted in the value of the initial bulk conductance of the SQ fiber (up to five times), but the influence of the latter on the output and transfer characteristics of the OFET was comparable. We explain this difference with the variation of the contact resistance at the gold/squaraine interface.

III. EXPERIMENTAL RESULTS AND DISCUSSION

Figure 2(a) displays the typical output characteristics for the SQ fiber OFET at different gate voltage applied. For $V_g = 0$, the dependence $I_d(V_d)$ characterizes the initial bulk conductance of the SQ fiber. For $V_d > 0$ and $V_g = 0$, holes are injected from the drain electrode, and only one polarity of charges is present in the bulk (inclusive the interface space where the accumulation channel appears at $V_g \neq 0$). We denote this current as I_b . For $V_d = 0$ and $V_g > 0$, Fig. 2(a) illustrates that the values of the measured current follow $I_d < 0$ and they depend on the gate voltage V_g . This fact can be explained with three processes which are active in the OFET. In correspondence with Fig. 1(c), for $V_d \neq 0$ and $V_g \neq 0$, three charge transport processes are active: (i) flow of holes from drain to source with density p_b , current I_b ; (ii) flow of electrons from source to drain with density n_s , current I_s ; (iii) leakage current $I_{le} = I_{dg} + I_{sg}$, where the first term is the current between drain and gate, and the second one the current between source and gate. In order to explain the negative values of I_d , we have measured the current-voltage ($I - V$) characteristics between drain and gate, and between source and gate. The resulting curves are given in the supplementary material (SI), Fig. S1. We found that the measured current $I_d \neq 0$ at $V_d = 0$ is comparable with the currents I_{dg} and I_{sg} , when the gate voltage amounts $V_g \neq 0$. The larger the voltage V_g , the larger is the leakage current I_{le} . In correspondence with the measuring circuit [Fig. 1(c)], for the similar sign of voltage V_d and V_g , the currents I_d and I_{dg} flow across the drain electrode in opposite direction. For $V_g = \text{const}$, the current I_{dg} is constant, and an increase of the positive voltage V_d leads to an increase of the hole density injected from drain. The corrected current between source and drain, I_{dk} , can be determined as $I_{dk} = I_d - I_{dg} = I_d - I_{d0}$, where I_d and

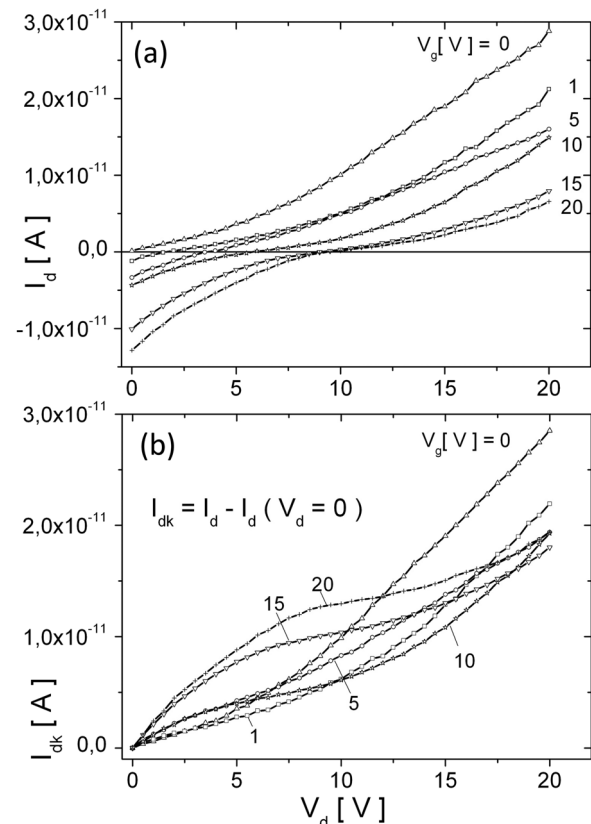


FIG. 2. (a) Measured output characteristics $I_d(V_d)$ at different gate voltage V_g . (b) Corrected output characteristics $I_{dk}(V_d)$ obtained from part (a).

I_{d0} are the values of the total measured current at $V_d \neq 0$ and $V_d = 0$, respectively. In other words, I_{dk} is a current between source and drain without influence of the leakage current. The resulting dependences of I_{dk} as a function of the positive voltage V_d at different V_g are shown in Fig. 2(b). In the following, we consider how the bulk current [$I_b = I_{dk}(V_g = 0)$] acts on the dependences $I_{dk}(V_d)$ measured between source and drain at different V_g .

Figure 2(b) demonstrates that all $I_{dk}(V_d)$ curves for $V_g = 1, 5, 10, 15$, and 20 V are characterized by three regimes, namely, linear, saturation, and of increasing saturation current at high V_d . In the opposite, the bulk current ($V_g = 0$) can be approximated by a power-law $I \sim V^\beta$ with the scaling exponent $\beta \approx 1$ for small and $\beta \approx 1.6$ for high voltage V_d (see Fig. S2 in supplementary material). The latter crosses all other curves for $V_g \neq 0$. The larger the voltage V_g , the larger is the voltage of the crossing point, V_{cr} . The crossing voltage V_{cr} lies about in the middle of the saturation range of each curve. It is evident that the output curves I_{dk} as function of V_d at different V_g are a superposition of the behavior of electrons injected from source and the behavior of holes injected from drain (bulk current).

For a more detailed analysis, we consider the interplay between two curves, namely, the curve of the bulk current ($V_g = 0$) and that one for the case $V_g = 15$ V, see Fig. 3.

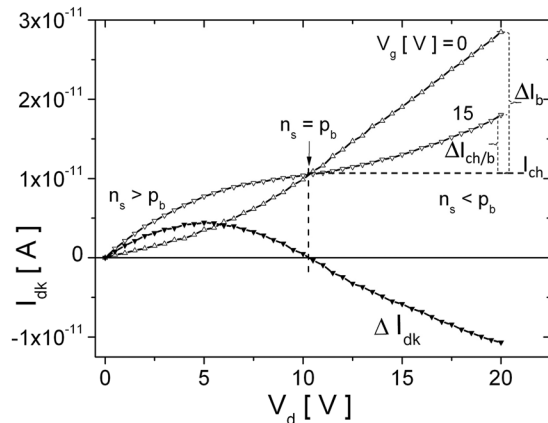


FIG. 3. Dependences $I_{dk}(V_d)$ at $V_g=15$ V and $V_g=0$ V [presented in Fig. 2(b)] and the corresponding difference ΔI_{dk} between both curves. The abbreviations I_{ch} , $\Delta I_{ch/b}$, and ΔI_b are explained in the text.

For positive drain and gate voltage, electrons are injected from source into the accumulation channel. The linear regime is observed, when a small source-drain voltage $V_d \ll V_g - V_{te}$ has been applied. Here, the electron density n_s injected from source is larger than the hole density p_b injected from drain, and the influence of the latter on the total $I - V$ curve is small. This fact can be clearly observed in Fig. 3, where the difference ΔI_{dk} between the curve for $V_g=15$ V and that one for $V_g=0$ V is presented. The inequality $n_s > p_b$ is valid up to the voltage V_{cr} . For the crossing point $V_d = V_{cr}$, the condition $n_s \approx p_b$ holds (assuming the similar mobility). The dominance of the hole density injected from drain is observed for the voltage range $V_d > V_{cr}$. That means, the initial bulk current of the SQ fiber determines its total $I - V$ curve and, moreover, causes the increase of the saturation current of the OFET. The hole injection from the drain always takes place when $V_d > 0$ is applied. It must be noted that the increase of the saturation current, in our case, is different compared with traditional ambipolar OFET,^{3,4} where the injection of the holes from the drain electrode only takes place in the drain voltage regime $V_d > V_g - V_{th}$. In our case, this process is small as it follows from the fact that the curve for the bulk current ($V_g = 0$) lies sufficiently above that for $V_g=15$ V.

Figure 4(a) illustrates the transfer characteristics at different voltage V_d , where the negative and positive parts of the drain current can be observed. For $V_d=0$, the curve $I_d(V_g)$ characterizes the leakage current. This fact can be clearly observed in the inset of Fig. 4(a), where the latter curve is compared with the curve $I_{dg}(V_g)$ measured between drain and gate. The corrected dependences $I_{dk}(V_g)$ for $V_d \neq 0$ can be determined from Fig. 4(a) as $I_{dk}(V_g) = I_d(V_g) - I_{dg}(V_g) = I_d(V_g) - I_d(V_g, V_d = 0)$. In other words, the dependence $I_{dk}(V_g)$ describes a current between source and drain as a function of the gate voltage without influence of the leakage current. The resulting dependences are presented in Fig. 4(b). They show that, for each curve $V_d = \text{const}$ and $V_g > 0$, the total current I_{dk} initially decreases due to the increase of the electron current

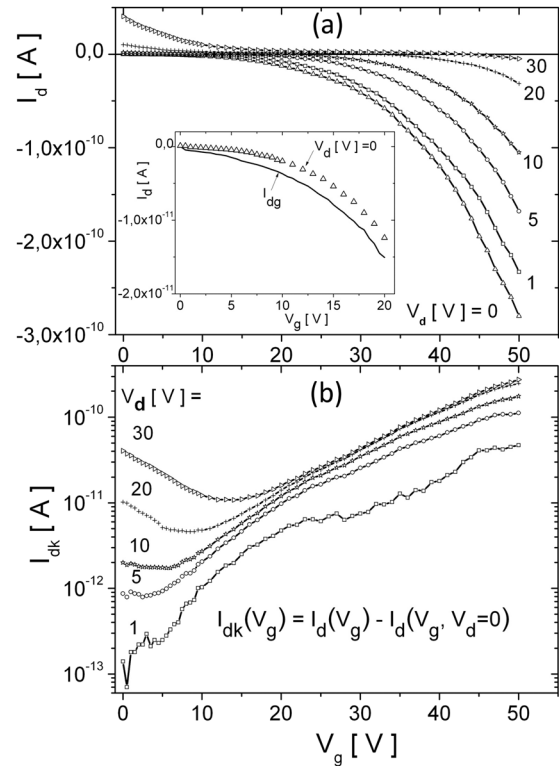


FIG. 4. (a) Measured transfer characteristics $I_d(V_g)$ at different drain voltage V_d . In inset: the currents I_{dg} and $I_d(V_d=0)$ as a function of V_g are presented. (b) Log plot of the corrected transfer characteristics evaluated from part (a).

in the accumulation channel, although the hole current in the bulk stays constant ($n_s < p_b$). After passing the minima at the gate voltage $V_g \approx 0.5V_d$ ($n_s \approx p_b$), the total current increases again due to the condition $n_s > p_b$. For a large voltage V_g , only electrons are located in the accumulation channel.

The mobility of electrons has been estimated from the linear regime of the device operation (in the range $V_d \ll V_g - V_{te}$) using Eq. (1) to

$$\mu_e = \frac{\partial I_{dk}}{\partial V_g} \times \frac{L}{WC_i V_d}, \quad (5)$$

where $C_i = 10\text{nF}/\text{cm}^2$. For this purpose, we have used the curve $I_{dk}(V_g)$ for $V_d=10$ V from Fig 4(b). The resulting value of the electron mobility amounts to $\mu_e = 7.2 \times 10^{-4} \text{ cm}^2/\text{Vs}$ (see Fig. S3 in supplementary material). The output and transfer characteristics for the case of $V_d < 0$ and $V_g < 0$ are similar with those presented above. The value of the hole mobility amounts to $\mu_h = 7.8 \times 10^{-4} \text{ cm}^2/\text{Vs}$ (see Fig. S4 in supplementary material). It should be noted that the values of the hole and electron mobility of all eight samples studied were found in the range between 10^{-4} and $10^{-3} \text{ cm}^2/\text{Vs}$. These values are in good agreement with those reported in Refs. 6, 11 for the ambipolar OFETs, but they are by far below the highest hole mobility ($1.3 \text{ cm}^2/\text{Vs}$) reported in Ref. 12 for the unipolar OFETs based on squaraines.

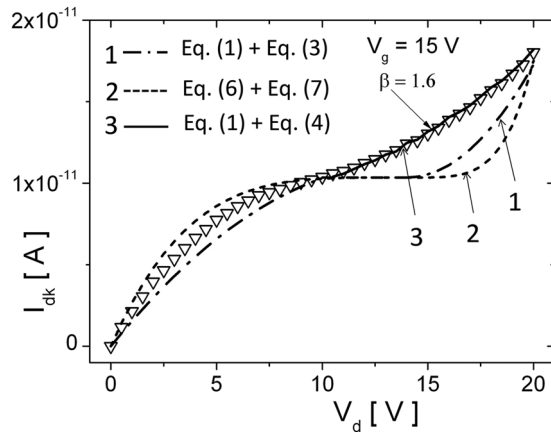


FIG. 5. Dependence $I_{dk}(V_d)$ at $V_g=15$ (redrawn from Fig. 3) and the corresponding fit lines. Line 1 is a fit due to Eq. (1) at small voltage V_d and Eq. (3) at large voltage V_d . Line 2 is a fit due to Eq. (6) at small voltage V_d and Eq. (7) at large voltage V_d . Line 3 is a fit due to Eq. (1) at small voltage V_d and Eq. (4) at large voltage V_d .

In order to describe the output characteristics $I_{dk}(V_d)$, as an example, we looked at $V_g=15$ V [Fig. 3]. First, we fitted this curve with the basic Eq. (1) at small voltage V_d and with Eq. (3) at high voltage V_d . Figure 5 presents the resulting fit (line 1), where the best fit parameters amount to $\mu_e = 1 \times 10^{-4}$ cm²/Vs, $V_{te}=1$ V, $\mu_h = 3.7 \times 10^{-4}$ cm²/Vs, and $V_{th}=-1$ V. The difference of the fit values of μ_e and μ_h compared to those evaluated experimentally can be explained with the determination accuracy of the latter [Eq. (5)]. The values $V_{te}=1$ V and $V_{th}=-1$ V are realistic, if we compare the output characteristics at $V_g=0$ and $V_g=1$ V in Fig. 2, where the applied gate voltage of 1 V leads to an essential increase of the source-drain current. That means, the threshold voltage for the electron accumulation amounts to $V_{te} \leq 1$ V.

Second, we fitted the same output characteristic $I_{dk}(V_d)$ at $V_g=15$ V with the model presented by Smits et al.,⁵ where the variable-range hopping in an exponential DOS was considered. For the linear regime of the OFET function ($0 \leq V_d < V_g - V_{te}$), the current in the accumulation channel is given by

$$I_d = \gamma_e \frac{W}{L} \frac{1}{a(a-1)} [(V_g - V_{te})^a - (V_g - V_{te} - V_d)^a], \quad (6)$$

and in the range of the ambipolar operation ($V_{te} \leq V_g - V_{th} \leq V_d$), it is given by

$$I_d = \frac{W}{L} [\gamma_e \frac{1}{a(a-1)} (V_g - V_{te})^a + \gamma_h \frac{1}{c(c-1)} (V_d - V_g + V_{th})^c], \quad (7)$$

where $a = 2T_{0e}/T$ and $c = 2T_{0h}/T$. T_{0e} and T_{0h} are the characteristic temperatures that indicate the widths of the exponential density of states for electrons and holes, respectively. γ_e and γ_h were considered in our work as fit parameters, but the details about them can be found in Ref. 5 The resulting fit is presented in Fig. 5 (line 2), where the best fit values amount to $\gamma_e = 3.1 \times 10^{-14}$, $\gamma_h = 4.0 \times 10^{-13}$, $V_{te}=1$ V, $V_{th}=-1$ V, $T_{0e}=592$ K, and $T_{0h}=650$ K. The values of γ_e , T_{0e} , and T_{0h} are comparable

with those reported for squaraine in Ref. 6, but the value of γ_h is about two orders larger than that reported in Ref. 6 The characteristic energy of the trap distribution for electrons is $k_B T_{0e}=0.05$ eV, and for holes $k_B T_{0h}=0.06$ eV. Here, k_B means the Boltzmann constant.

Third, we fitted the same output characteristic $I_{dk}(V_d)$ at $V_g=15$ V with the standard Eq. (1) at small voltage V_d and with Eq. (4) at high voltage V_d (line 3). The determination of the fraction α of the bulk current in the total measured current is explained in Fig. 3, where I_{ch} indicates the saturation current of the curve $I_{dk}(V_d)$ at $V_g=15$ V. The difference between the saturation curve I_{ch} and that of $I_{dk}(V_d)$ at $V_g=15$ V is denoted as $\Delta I_{ch/b}$, the difference between the curve I_{ch} and that of $I_{dk}(V_d)$ at $V_g=0$ V (bulk) as ΔI_b . It is evident that both parameters $\Delta I_{ch/b}$ and ΔI_b depend on the drain voltage V_d . The parameter α is determined as $\alpha = \Delta I_{ch/b}/\Delta I_b$, and, consequently, depends on the voltage V_d . For the exponent value $\beta=1.6$, Fig. 5 presents the resulting fit, where the best fit parameters amount $\mu_e = 1 \times 10^{-4}$ cm²/Vs, $V_{te}=1$ V, and $b = 1.8 \times 10^{-13}$ A. Upon comparing all three fit lines presented in Fig. 5, it is evident that Eq. (4) with $\beta=1.6$ achieves best agreement with the experimental results as compared to the same obtained with Eq. (3) and Eq. (7). That means, the bulk conductance of the SQ fiber in the OFET studied caused the increase of the saturation current in the unipolar transistor.

IV. CONCLUSIONS

We have studied a field-effect transistor based on a squaraine fiber fabricated via self-assembled crystallization of SQ molecules on a glass substrate. Our experiments have demonstrated that the initial bulk conductance of the fiber was comparable with the conductance of the accumulation channel in the OFET as well as with the leakage conductance between drain (source) and gate. The measured total output and transfer $I - V$ characteristics are a result of the superposition of these three currents. Depending on the ratio between drain voltage V_d and gate voltage V_g , one of the three currents becomes dominant. We provide evidence how these three currents can be separated. The output characteristics clearly feature three different regimes, namely, linear, saturation, and of increasing saturation current at large V_d . We found that the bulk conductance of the SQ fiber in the OFET described by the law $I_d \sim V_d^{1.6}$ leads to the increase of the saturation current of the device operation approximated by Eq. (4) with the exponent $\beta=1.6$.

SUPPLEMENTARY MATERIAL

See [supplementary material](#) for the complete description of the influence of the bulk conductance on that one of the accumulation channel of the unipolar field-effect transistor.

REFERENCES

- 1 E. J. Meijer, D. M. de Leeuw, S. Setayesh, E. van Veenendaal, B. H. Huisman, P. W. M. Blom, J. C. Hummelen, U. Scherf, and T. M. Klapwijk, *Nat. Mater.* **2**, 678 (2003).
- 2 A. Facchetti, *Mater. Today* **10**, 28 (2007).

- ³R. Schmechel, M. Ahles, and H. von Seggern, *J. Appl. Phys.* **98**, 084511 (2005).
- ⁴J. Zaumseil and H. Siringhaus, *Chem. Rev.* **107**, 1296 (2007).
- ⁵E. C. P. Smits, T. D. Anthopoulos, S. Setayesh, E. van Veenendaal, R. Coehoorn, P. W. M. Blom, B. de Boer, and D. M. de Leeuw, *Phys. Rev. B* **73**, 205316 (2006).
- ⁶E. C. P. Smits, S. Setayesh, T. D. Anthopoulos, M. Buechel, W. Nijssen, R. Coehoorn, P. W. M. Blom, B. de Boer, and D. M. de Leeuw, *Adv. Mater.* **19**, 734 (2007).
- ⁷G. D. Wei, X. Xiao, S. Y. Wang, J. D. Zimmerman, K. Sun, V. V. Diev, M. E. Thompson, and S. R. Forrest, *Nano Lett.* **11**, 4261 (2011).
- ⁸L. V. Govor, G. H. Bauer, and J. Parisi, *Rev. Sci. Instrum.* **81**, 106108 (2010).
- ⁹S. Wang, E. I. Mayo, M. D. Perez, L. Griffe, G. Wei, P. I. Djurovich, S. R. Forrest, and M. E. Thompson, *Appl. Phys. Lett.* **94**, 233304 (2009).
- ¹⁰G. Chen, D. Yokoyama, H. Sasabe, Z. Hong, Y. Yang, and J. Kido, *Appl. Phys. Lett.* **101**, 083904 (2012).
- ¹¹P. H. Wöbkenberg, J. G. Labram, J.-M. Swiecicki, K. Parkhomenko, D. Sredojevic, J.-P. Gisselbrecht, D. M. de Leeuw, D. D. C. Bradley, J.-P. Djukic, and T. D. Anthopoulos, *J. Mater. Chem.* **20**, 3673 (2010).
- ¹²M. Gsänger, E. Kirchner, M. Stolte, C. Burschka, V. Stepanenko, J. Pflaum, and F. Würthner, *J. Am. Chem. Soc.* **136**, 2351 (2014).